Calculations of high-pressure properties of beryllium: Construction of a multiphase equation of state

Lorin X. Benedict, Tadashi Ogitsu, Andrea Trave, Christine J. Wu, Philip A. Sterne, and Eric Schwegler
Condensed Matter and Materials Division, Physical and Life Sciences Directorate, Lawrence Livermore National Laboratory, Livermore, California 94550, USA

(Received 24 July 2008; revised manuscript received 24 September 2008; published 11 February 2009)

We describe the construction of a three-phase equation of state for elemental beryllium. The phases considered are: the ambient hcp phase, the high-temperature bcc phase, and the liquid. The free energies of the solid phases are constructed from cold, ion-thermal, and electron-thermal components derived from *ab initio* electronic structure-based calculations. We find that the bcc phase is unstable near ambient conditions and that even at high pressures at which the bcc phase is stable, the bcc-hcp energy barrier can be as small as a few hundred kelvins. The liquid free energy is based on a model of Chisolm and Wallace and is constrained by using the melt curve (determined by *ab initio* two-phase simulations) as a reference. The high-temperature plasma limit is addressed with an average-atom-in-jellium model. Comparisons to experimental results, both for the ambient hcp phase and for the phase diagram as a whole, are discussed.

DOI: 10.1103/PhysRevB.79.064106 PACS number(s): 81.30.Bx, 91.60.Fe, 91.60.Gf, 91.30.Mv

I. INTRODUCTION

Even after a few decades of research,[1] the phase diagrams of elemental metals in the multimegabar range still constitute a field of active fundamental investigation.[2] Much of this is due to the myriad experimental difficulties associated with achieving and maintaining such pressures, together with the paucity of diagnostic techniques capable of determining phase information at ultrahigh P and T. On the theoretical side, the major challenge is the development of first-principles methods which are able to reproduce (or indeed, predict) free energy differences between competing phases in instances where these differences decrease significantly as pressure is increased.[3] This is a special challenge in closed-packed metals, where energy differences between, for instance, bcc and hcp phases can be extremely small even at moderate pressures where continuous transformations between such structures are possible.[4]

Beryllium is one such element that falls squarely into the category of a poorly understood closed-packed metal. As we shall discuss, its competing solid phases are extremely close in energy throughout a wide range of compressions, and there exist transformation paths between these phases which have been predicted to give rise to mechanical instabilities near ambient conditions.[5,6] In addition, beryllium has recently received considerable attention as a possible ablator material for fuel capsules to be used in inertial confinement fusion experiments.[7] The engineering design of these capsules is based on large-scale hydrodynamic simulations,[8] which model the behavior of the materials at the extreme temperatures and pressures of the experiment. In order to close the set of hydrodynamic equations, it is necessary to introduce the equation of state (EOS) of the material, which in turn depends on its phase (solid, liquid). It is therefore of crucial importance to know the phase diagram of the system, denoting which phase is thermodynamically stable in a given set of pressure and temperature conditions.[9] Information about EOS and the phase diagram should, where possible, be obtained directly from experiment. However, many conditions of interest are outside the range where highly accurate thermodynamic data are available. It is then often necessary to rely on theoretical predictions of EOS, which again are related to theoretical predictions of the phase diagram in these extreme conditions.

Even at temperatures below melting and at pressures below 100 GPa, the phase diagram of beryllium is still quite poorly known. At ambient pressure and temperature, hcp Be is known to possess a nonideal c/a ratio. When heated at ambient pressure, experiments[10] have detected a solid-solid phase transition to what is believed to be a bcc structure in a narrow range of temperature prior to melting. These experiments suggest that the hcp-bcc phase boundary has a negative slope, while subsequent work suggests that it may be positive.[11] The conflicting observations have motivated numerous research efforts to search for a possible pressure-driven transition at room temperature. While theoretical calculations have provided a large range of pressures at which this transition may happen, no experiments (up to 300 GPa) have yet found any evidence of it.[12,13] In addition, more recent diamond-anvil-cell x-ray measurements have failed to find any evidence for a bcc phase for temperatures between 300 and 2000 K, and pressures between 15 and 50 GPa.[13]

Recent theoretical studies aimed at determining the hcp-bcc phase line[5,6,14,15] throughout a wide range of temperatures have employed *ab initio* electronic structure calculations to constrain phase-dependent free energy models which include cold compression, quasiharmonic ion-thermal, and (deemed negligible here) electron-thermal contributions. By using a standard form for the quasiharmonic ion-thermal contribution[17] constrained by *ab initio* phonon density-of-states (PDOS) results together with cold and electron-thermal pieces, Rudin *et al.*[5] obtained an hcp-bcc transition temperature well above that inferred from experiment. Robert *et al.*[14] obtained a similar result from their nearly equivalent *ab initio* calculations and showed that roughly a 30% reduction in the bcc Debye temperature would be needed to bring the extrapolation of the ambient-pressure hcp-bcc transition temperature below the melt line. Kadas *et al.*[15] argued

that the presence of the bcc phase seen in the early experiments[10,11] could be explained by an electronic topological transition, in which the elastic constants of the bcc phase are softened greatly due to Fermi-surface nesting effects. In these works, the authors pointed out the possibility that the bcc phase could exhibit large anharmonic effects which could affect the transition line substantially, a point motivated by the instability of bcc Be near ambient conditions due to a soft phonon mode.[5,6,14,15]

In this study, we construct a three-phase EOS for Be, paying particular attention to the accurate prediction of the hcp-bcc phase line. In support of this, we perform $T=0$ *ab initio* total-energy calculations along the so-called Burgers path, connecting bcc to hcp, in which we find the energy barrier between hcp and bcc to be very small (well below $k_B T_{\mathrm{melt}}$). The free energy of the liquid phase is taken to be of the form suggested by Chisolm and Wallace[16] and is constrained by requiring that the solid-liquid phase line is that as obtained by *ab initio* two-phase simulations,[26] together with Wallace's assumption of a latent heat which is independent of compression.[3,17] The very high-T limit, in which inner-shell ionization occurs and the resulting electron-thermal free energy is pronounced, is addressed by connecting to the results of Purgatorio,[18] a density-functional theory (DFT)-based average-atom-in-jellium model. Our multiphase EOS for Be exhibits an hcp-bcc-liquid triple point at ~180 GPa and 4500 K and a principal shock Hugoniot which possesses a small portion in the bcc-stable region. We predict no thermodynamically stable bcc phase below $P \sim 180$ GPa, in agreement with previous predictions[5,6,14] but in contrast to earlier experiments.[10,11] Comparisons to available experimental results are discussed.

II. CONSTRUCTION OF hcp AND bcc FREE ENERGIES

We make the fundamental assumption that the Helmholtz free energy (E-TS) for each phase can be decomposed into a sum of three independent terms,

$$F(V,T) = F_0(V) + F_i(V,T) + F_e(V,T), \tag{1}$$

where F_0 represents the total energy of the system at $T=0$ with *fixed* ionic positions, F_i is the thermal contribution from ionic motion together with the free energy due to zero-point motion, and F_e represents the thermal contribution from excited electrons. All calculations we perform to construct the above terms are based on self-consistent electronic structure theory using the generalized gradient approximation (GGA) within DFT as parametrized by Perdew-Burke-Ernzerhof.[19] We compute $F_0(V)$, henceforth called the cold curve, of each phase using both plane-wave pseudopotential[20] and linear muffin-tin orbital all-electron methods. Ground-state energies were computed over a range of pressures from 0 to 1400 GPa. A plane-wave energy cutoff of 60 Ry was used throughout all of our pseudopotential calculations. A k-point mesh of $24\times24\times15$ in the full Brillouin zone was used for hcp, while a $24\times24\times24$ mesh was used for bcc. The Be pseudopotential was chosen to be of the Troullier-Martins type[21] using the Kleinman-Bylander separable form[22] with s,p-nonlocal and d-local channels and a matching radius of 0.7938 Å. At each pressure, internal cell parameters were optimized. While bcc can be described by just one parameter (chosen to be the size of the cubic cell), hcp requires two parameters: a describing the size of the hexagons in the close-packed layers and c the distance between them. For convenience, hcp has been represented with an orthorhombic supercell which corresponds to twice its elemental cell. Below a volume of 3.6 Å^3/atom ($P>400$ GPa), we use the all-electron method to obtain ground-state energies; at intermediate volumes, we find the results of our pseudopotential calculations to be in good agreement with the all-electron computations.

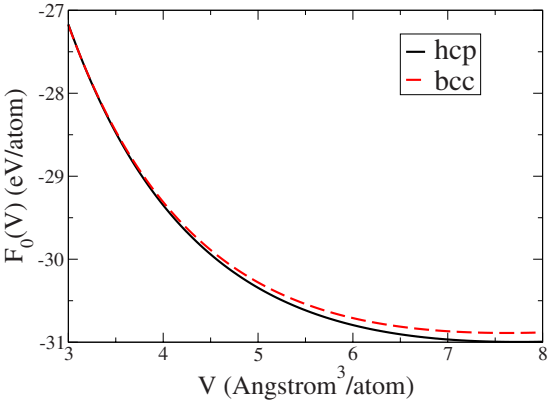

FIG. 1. (Color online) Vinet fits (Ref. 23) to cold curves for hcp (solid) and bcc (dashed) Be.

A. Internal energies at $T=0$

Up to roughly 400 GPa, hcp has a lower energy than bcc. Figure 1 shows our computed hcp and bcc cold curves, presented as continuous functions of V by fitting using the form of Vinet *et al.*,[23]

$$F_0(V) = \frac{4V_0B_0}{(B_1-1)^2}[1-(1+X)\exp(-X)] + \phi_0, \tag{2}$$

where ϕ_0 is the minimum energy and

$$X = \frac{3}{2}(B_1-1)[(V/V_0)^{1/3}-1]. \tag{3}$$

We obtain the fit parameters: $V_0(\mathrm{hcp})=7.751$ Å^3/atom, $B_0(\mathrm{hcp})=111.5$ GPa, and $B_1(\mathrm{hcp})=3.69$; $V_0(\mathrm{bcc})=7.618$ Å^3/atom, $B_0(\mathrm{bcc})=116.7$ GPa, and $B_1(\mathrm{bcc})=3.64$, together with an energy difference between their respective energy minima of $E_0^{\mathrm{bcc}}-E_0^{\mathrm{hcp}}=0.108$ eV/atom.[24] Note that at each volume, the energy difference between the phases is remarkably small, as noted by others.[5,6,14] The pressure-volume relation (containing information about equilibrium volumes and bulk moduli) and the dependence of the hcp c/a ratio on pressure can be compared with diamond-anvil-cell experiments. The equilibrium density and structural parameters of the hcp phase at ambient conditions are in good agreement with values published in the literature. We compare these values in the next section, after we have accounted for the effects of zero-point motion and thermal expansion. For now, we note

that in agreement with previous theoretical work[5,6,25] and experimental results,[12] we find that the c/a ratio of hcp Be has the small value of 1.57 at ambient pressures and rises gradually toward the ideal value of 1.633 at higher pressures.

Motivated by *ab initio* molecular dynamics (MD) studies of Be melting,[26] in which bcc and hcp phases of Be were seen to transform into each other rather readily at certain high-T conditions, we chose to study the energetics of possible transformation paths between them. Clearly defined transformation paths exist between simple crystal structures, such as the Bain path connecting bcc and fcc (Ref. 27) and the Burgers path connecting bcc and hcp.[28] In several elements, the existence of these paths leads to martensitic transitions, that is, phase transformations that occur as a collective change in the whole sample rather than by nucleation. It is possible to analyze intermediate structures along these paths as a means to understand the relative stability of the phases and the existence of potential barriers hindering the transitions. In conducting these studies, it is necessary to achieve an extremely high degree of convergence with respect to the representation of the single-electron wave functions in terms of plane waves and the k-point sampling of these wave functions. Poorly converged results can dramatically affect the shape of these potential surfaces and artificially distort structures from their equilibrium. We chose an energy cutoff of 120 Ry and a k-point mesh for the four-atom rhombohedral cell of $24\times24\times24$ for this part of our work. This ensures that our energies are converged to within 0.1 meV/atom (corresponding to a temperature of 1.16 K) and our pressures to within 0.005 GPa.

The Burgers path,[28] connecting bcc to hcp, consists of two separate distortions: a shear deformation consisting of a compression along $\langle 100\rangle_{\mathrm{bcc}}$ and an elongation along $\langle 110\rangle_{\mathrm{bcc}}$, and a relative shuffling of $\langle 100\rangle$ planes, corresponding to the T_1 N-point phonon mode of the bcc lattice.[4] This transformation can be best represented by choosing a tetragonal cell for bcc containing four atoms, with $a=b=\sqrt{2}c, c$ being the side of the conventional cubic cell. In this reference cell, $\langle 100\rangle$ planes will become, after the shear deformation, the hexagonal layers of hcp. The relative shuffling of the hexagonal layers is represented by a displacement parameter δ, defined to be the (unitless) relative amplitude of the T_1 N-point phonon (see Ref. 4 for details). The angle between [111] directions is denoted by α. For the hcp structure, $\alpha=120°$, while for bcc, $\alpha=109.47°$. Deformation of this type brings the system to an hcp structure characterized by $c/a=1.57$, smaller than the ideal value of 1.633. Additional distortions can be made which allow for different c/a ratios, but we chose to fix this value for this part of the study (since this is essentially equal to the equilibrium value we found at ambient conditions) and compute the total energy as a function of (δ,α) at several volumes. Figure 2 shows the ground-state total-energy difference for Be at $T=0$ as a function of δ and α for $V=7.63$ Å^3/atom ($P\sim0$ GPa). The energy surface possesses a minimum at hcp, while in the neighborhood of bcc, the magnitude of the energy is higher and the surface is quite flat. In particular, there is no barrier preventing bcc from transforming directly into hcp. This instability of bcc Be near ambient pressures was recognized by others previously in the context of *ab initio* phonon calculations,[5,6] in which imaginary phonon frequencies were computed at low pressures. We note here that *even at higher pressures at which bcc is mechanically stable, the energetic barrier between bcc and hcp along the Burgers path can be exceptionally small*. This is illustrated in Fig. 3, which shows one-dimensional (1D) projections of the Burgers energy surface in which α is varied and δ is chosen to give the lowest energy for each α. Two volumes are shown: $V=7.63$ ($P\sim0$) and 3.75 Å^3/atom ($P\sim300$ GPa). Note that for $V=3.75$ Å^3/atom, bcc ($\alpha=109.47°$) is indeed metastable, as also demonstrated by phonon calculations, but the energy barrier is rather small, which is ~400 K, far lower than the melt temperature at this pressure. In addition, we have found that the shape of the energy well around bcc is very flat at all compressions (less so for hcp; see the 1D profile of the well around $\alpha=120°$ in Fig. 3), suggesting that anharmonicity may be crucially important in bcc Be. One notable observation is that the small nonideal value for the hcp c/a ratio at low pressure may actually facilitate deformation along the Burgers path because it is precisely this low value which is required to move from hcp to bcc with minimal additional distortions.[28]

In constructing the free energy of solid Be, we assume that the individual hcp and bcc phases remain distinct even at

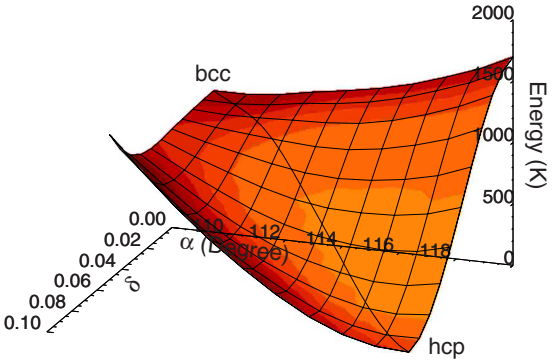

FIG. 2. (Color online) Ground-state energy difference (neglecting zero-point motion) $E(\alpha,\delta)-E_{\mathrm{hcp}}$ in kelvin for Be along the two-dimensional plane of parameters (α,δ) describing the Burgers path for $V=7.63$ Å^3/atom.

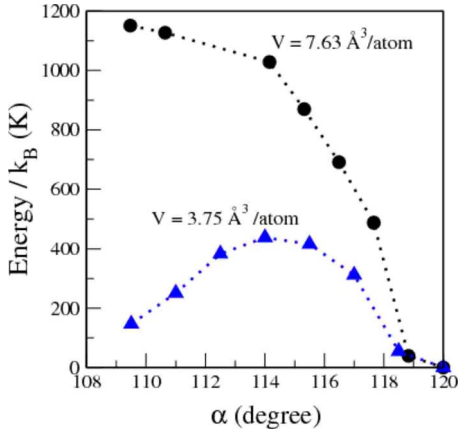

FIG. 3. (Color online) Ground-state energy difference (neglecting zero-point motion) of Be along a 1D slice through the two-dimensional Burgers path for $V=7.63$ and 3.75 Å^3/atom.

temperatures above which transformations such as that suggested by Fig. 3 could occur. The reasons are twofold. (1) The Burgers transformation represents *an individual mode of ionic excitation*. In a heated solid, only a tiny fraction of the thermal energy will be distributed to this particular mode. Other modes are expected to leave the system in a distinct solid phase as long as the amplitudes are small (i.e., for $T < T_{melt}$). (2) Even if the energy barrier in question is overcome, we will show below that the EOSs of hcp and bcc are remarkably similar. Though the entropy of the solid may be slightly affected by an increased propensity for Be to visit intermediate states between hcp and bcc along the Burgers path, the internal energy and pressure will likely be rather insensitive to these infrequent excursions, given the very small energy differences we see in Fig. 3.

B. Ion-thermal free energy: Quasiharmonic theory

In order to investigate the free energy due to thermal motion of the ions, we compute the free energy within quasiharmonic theory[29] for each solid phase. From the volume-dependent PDOS, $D_V(E)$, the harmonic free energy due to zero-point motion and thermal occupation of the independent normal modes is[29]

$$F_i(V,T) = 3\int_0^\infty dE D_V(E) \times \left[\frac{1}{2}E + k_B T \log[1-\exp(-E/k_B T)]\right]. \quad (4)$$

At temperatures larger than the characteristic phonon energies, this reduces to the familiar Mie-Grüneisen ion-thermal contribution, $F_i(V,T)=3k_BT\log[\theta_0(V)/T]$, where θ_0 is the logarithmic moment of the PDOS, defined by

$$k_B\theta_0(V) = e^{1/3}\exp\left(\int \log(E) D_V(E) dE\right). \quad (5)$$

As $T\to 0$, $F_i(V,T)\to \frac{9}{8}k_B\theta_1(V)$, where θ_1 is the first frequency moment of the PDOS, defined by

$$k_B\theta_1(V) = \frac{4}{3}\int E D_V(E) dE. \quad (6)$$

Both moments are defined in such a way that if the PDOS is of the Debye form, in which $D_V(E)\propto E^2$ for $E<k_B\theta(V)$ and is zero for $E>k_B\theta(V)$, then the moments are equal to each other and are equal to the Debye temperature, $\theta(V)$. In this case, the harmonic free energy may be written in terms of the single volume-dependent parameter $\theta(V)$,

$$F_i(V,T) = k_BT\left\{\frac{9}{8}\frac{\theta(V)}{T} + 3\log\{1-\exp[-\theta(V)/T]\} - \mathcal{D}[\theta(V)/T]\right\}, \quad (7)$$

with

$$\mathcal{D}(y) = \frac{3}{y^3}\int_0^y \frac{x^3}{\exp(x)-1}. \quad (8)$$

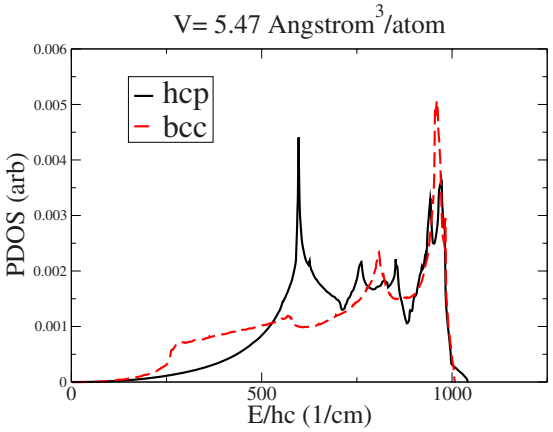

FIG. 4. (Color online) Phonon density of states of hcp (solid) and bcc (dashed) Be at $V=5.47$ Å^3/atom.

We have computed the PDOS on a dense grid of volumes (between $V=3$ and 8 Å^3/atom) for hcp and bcc phases using DFT-based linear response methods.[30] For bcc at large volumes, $V>7.67$ Å^3/atom, we compute a small number of imaginary phonon frequencies, indicating that bcc Be is mechanically unstable in these conditions.[5,6] This renders our calculations of phase stability meaningless in these cases. However in the interest of extrapolating into the unstable region, we ignore the contributions from imaginary frequencies in the PDOS by setting their spectral weight equal to zero in what follows. We stress that this is merely for convenience; in the end, we focus primarily on the region in which bcc is predicted to be metastable. Figure 4 shows $D_V(E)$ for both hcp and bcc at $V=5.47$ Å^3/atom. Note that both spectra possess large-intensity peaks at a wave number just below 1000 cm^{-1}, above which the intensity drops to zero. We find that large-energy high-intensity peaks coincide for both phases throughout the range of volumes of interest. This renders the various volume-dependent moments, discussed above, to be quite similar for the two phases. Though less apparent from the figure, it is also the case that for each phase we find θ_0 to be within 2% of θ_1 at all volumes. Therefore, the Debye model [Eqs. (7) and (8)] is an excellent approximation to the full quasiharmonic free energy [Eq. (4)]. Indeed, direct comparisons between the free energies of Eq. (4), using the full PDOS, and Eqs. (7) and (8), using a Debye temperature set equal to θ_0, bear this out. This is fortunate because one must differentiate $F_i(V,T)$ with respect to V to obtain the ion-thermal contribution to the pressure; it is much easier to characterize the volume dependence of a single number, θ, than the volume dependence of a whole function of energy, $D_V(E)$. To this end, we parametrize the V dependence of θ by assuming that the ion-thermal Grüneisen parameter varies linearly with V: $\gamma\equiv -d\log\theta/d\log V = AV+B$. This produces a three-parameter form for $\theta(V)$,

$$\theta(V) = \theta^{(0)}\left(\frac{V}{V_{\rm ref}}\right)^{-B}\exp[A(V_{\rm ref}-V)], \quad (9)$$

which we then fit to our *ab initio* calculations of θ_0 at various V for hcp and bcc Be. Choosing reference volumes of $V_{\rm ref}$(hcp)$=7.75$ Å^3/atom and $V_{\rm ref}$(bcc)$=7.62$ Å^3/atom, we

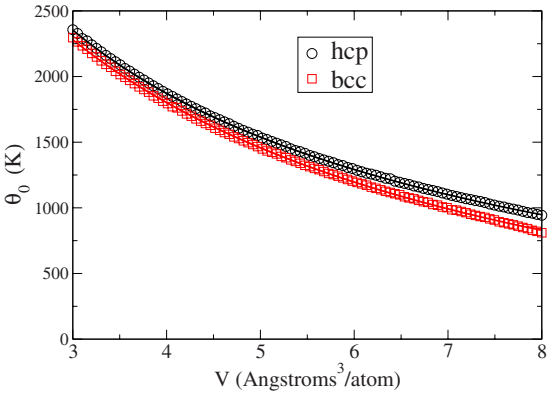

FIG. 5. (Color online) Computed θ_0 of hcp (open circles) and bcc (open squares), together with fits defined by Eq. (9) (solid lines).

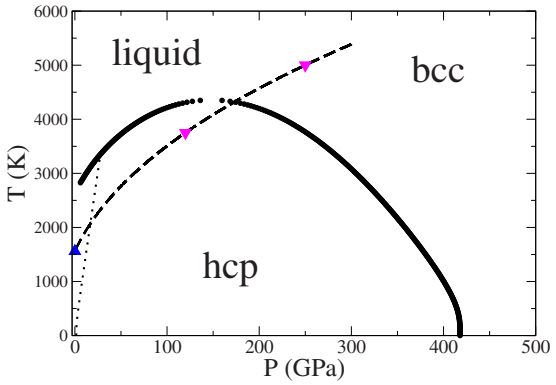

FIG. 6. (Color online) hcp-bcc phase line as computed from quasiharmonic theory. Also included is the melt curve (dashed line) inferred from a combination of experiments (upward triangle; Ref. 10) and calculations (downward triangles; Ref. 26). The dotted line denotes the isochore (in the bcc phase) for $V=7.67$ Å^3/atom. For $V>7.67$ Å^3/atom, corresponding to (P,T) points to the left of this line, bcc is predicted to be mechanically unstable.

obtain $\theta^{(0)}(\mathrm{hcp})=982.8$ K, $A(\mathrm{hcp})=0.081$ Å^{-3}, $B(\mathrm{hcp})=0.515$; $\theta^{(0)}(\mathrm{bcc})=886.9$ K, $A(\mathrm{bcc})=0.131$ Å^{-3}, and $B(\mathrm{bcc})=0.364$. This fit reproduces the computed values of $\theta^{(0)}$ to within 2% for both phases. Figure 5 shows the resulting $\theta(V)$ for hcp and bcc phases. Again, we stress that for $V>7.67$ Å^3/atom, the bcc $\theta(V)$ is an extrapolation which ignores the imaginary frequencies indicating mechanical instability for that phase.

We note in passing that the electron-thermal term of Eq. (1) has been shown to be small in solid Be.[5,6,14] Upon calculating the electronic densities of states for hcp and bcc Be as a function of V and using the low-T Sommerfeld expansion,[29] we too arrive at the conclusion that electronic excitations are of negligible importance for determining the hcp-bcc phase line. In particular, we find that the inclusion of electronic excitations changes the hcp-bcc transition temperature by not more than 5% even at the highest temperatures. Nevertheless, we do include electronic excitations (as inferred from our GGA-DFT calculations of the electronic density of states) in this work: invoking the Sommerfeld expansion, in which $F_e(V,T)\propto N(E_F)T^2$ at low T $(T<T_F)$, we take $F_e(V,T)=\alpha_e(V/V_e)^K T^2$.[29] Calculations of the V-dependent electronic densities of states then give $\alpha_e(\mathrm{hcp})=8.33\times10^{-6}$ K^{-2}, $K(\mathrm{hcp})=0.67$, $V_e(\mathrm{hcp})=7.751$ Å^{-3}/atom, $\alpha_e(\mathrm{bcc})=1.57\times10^{-5}$ K^{-2}, $K(\mathrm{bcc})=0.86$, and $V_e(\mathrm{bcc})=7.618$ Å^{-3}/atom.

This treatment of cold+quasiharmonic ion-thermal +(very small) electron-thermal free energy contributions for solid Be produces excellent agreement with EOS data for the hcp phase. Recent measurement of the room-T isotherm[12] gives $B_0(\mathrm{hcp})=109.88$ GPa and $B_1(\mathrm{hcp})=3.59$, while our hcp equation of state gives $B_0(\mathrm{hcp})=104.58$ GPa and $B_1(\mathrm{hcp})=3.63$ at $T=300$ K. Our equilibrium volume at room T is 7.939 Å^3/atom, roughly 2% smaller than the measured value. Our computed (linear) thermal-expansion coefficient for hcp Be is $\alpha=10.9\times10^{-6}$ K^{-1}, compared to the experimental value of 11.3×10^{-6} K^{-1}.[31]

Because $\theta_{\mathrm{bcc}}(V)<\theta_{\mathrm{hcp}}(V)$ while the $T=0$ internal energy of hcp is less than that of bcc (for pressures below ~400 GPa), Be is predicted to undergo a transition from hcp→bcc as T is increased. Other researchers have predicted this as well.[5,6,14] By using the two-phase Maxwell construction with our phase-dependent Helmholtz free energies we compute the hcp-bcc phase line shown as the black curve in Fig. 6. The dotted line denotes the $V=7.67$ Å^3/atom isochore in the bcc phase. For $V>7.67$ Å^3/atom, bcc Be is predicted to be mechanically unstable at $T=0$ (discounting zero-point motion); all points to the left of the dotted line are therefore extrapolations into the bcc-unstable region.[32] Note that the *extrapolated* transition temperature between hcp and bcc at $P=0$ is 2630 K, significantly higher than the 1523 K result inferred from experiments and well above the ambient-pressure melt temperature of 1562 K.[10] Our current best estimate of the Be melt line appears as the dashed line in Fig. 6; the symbols represent the experimental $P=0$ melting point (upward triangle) and *ab initio* two-phase melting results (downward triangles) in which the solid phase is chosen to be bcc.[26] These three melt points are connected using a Simon-Glatzel fit.[33] Our hcp-bcc phase line result seems to be in reasonable agreement with the work of Rudin *et al.*[5] and Robert *et al.*,[14] though neither groups reported their extrapolated ambient-pressure hcp-bcc transition temperature. It is important to note that the hcp-bcc internal energy difference at $T=0$, giving rise to the cold hcp-bcc transition pressure of ~400 GPa,[5,6,14] is essentially within the typical errors associated with local density approximation (LDA) and/or GGA approximation. In this sense, errors in the cold energies could give rise to appreciable shifts in the phase boundary. In spite of this, we assume, for sake of argument, that the cold curves are sufficiently accurate for our purposes.

Yet another cause for concern is the complete neglect of anharmonicity, contributions to the energy of ionic excitations which are not merely quadratic functions of atomic displacements away from equilibrium. Anharmonicity can give rise to deviations of the specific heat from the Dulong-Petit value of $3k_B$/atom at high T. Large anharmonicity may be expected in situations in which barriers between local minima in the potential energy surface of the ions are small and can therefore be overcome at high T, such as shown in Fig. 3. Indeed, other groups have suggested this as a strong

possibility for bcc Be, owing to its mechanical instability at large V.[5,6] Our investigations using *ab initio* MD (described in detail below for its application to the liquid) have revealed only very minor deviations in the specific heat for both solid phases at the conditions relevant for their metastability.[34] We thus neglect anharmonicity in the construction of the solid free energies.

III. CONSTRUCTION OF LIQUID FREE ENERGY AND PHASE DIAGRAM

We break the modeling of the liquid EOS into two parts. The low-T ($k_BT<2$ eV) liquid free energy is constructed by using our solid free energies as a reference, together with our (limited) knowledge of the melt curve. The liquid EOS so constructed is then validated by performing select *ab initio* molecular dynamics calculations of the internal energy and pressure, which are shown to compare well to those of the model. The high-T ($k_BT>2$ eV) liquid free energy is constructed using a global EOS model similar to Quotidean equation of state (QEOS).[39] This is fit as closely as possible to the low-T EOS at $k_BT=2$ eV. At higher temperatures, where the electron-thermal term of Eq. (1) is dominant, this approach uses an atom-in-jellium model known as Purgatorio[18] to describe ionization due to pressure and temperature.

A. Low-T liquid

For an elemental metallic liquid at temperatures in the neighborhood of melting, the specific heat is generally quite close to the Dulong-Petit value of $3k_B$/atom, just as it is for solids.[3] As such, it is reasonable to assume that the liquid free energy can be modeled in a manner similar to that for solids. We use the model of Chisolm and Wallace,[16] in which the free energy per atom is of the form

$$F(V,T) = F_0(V) + 3k_BT\log\left(\frac{\bar{\theta}}{T}\right) - k_BT\log(w) + F_e(V,T). \tag{10}$$

The first term is a "cold curve" for the liquid. The second term is a Mie-Grüneisen piece accounting for ionic excitations at high T within a representative many-body potential well with a curvature set by the effective Debye temperature, $\bar{\theta}$. The third term accounts for the presence of multiple such wells (with the number of wells being w^N, where N is the number of atoms) and can be combined with the second term by defining another effective Debye T, $\tilde{\theta}=\bar{\theta}/w^{1/3}$. The last term accounts for electronic excitations. This form for the liquid free energy has specific heat $C_V=3k_B$/atom if $F_e=0$. It was shown previously by some of us that this form works very well in reproducing both melt lines and liquid EOS calculations for liquid carbon.[35]

Since the electron-thermal term is of negligible importance for the solid phases of Be, we also expect it to be relatively unimportant for the liquid (for this low-T part). This will be justified below when comparing to *ab initio* calculations. For convenience (see below), we then fix the electron-thermal term for the liquid to be exactly the same as for the bcc phase. Hence, $F_e(V,T)=\alpha_e(V/V_e)^KT^2$, where K(liquid)$=0.67$, V_e(liquid)$=7.751$ Å^{-3}/atom, and α_e(liquid) $=1.57\times10^{-5}$ K^{-2}. Just as for the hcp-bcc phase line, we find the melt lines to be practically unaffected by setting $F_e=0$ for all three phases. The parameters of the liquid model are then completely specified by $F_0(V)$, which controls the energy difference between solid and liquid, and $\tilde{\theta}(V)$, which controls the entropy difference.

We first consider $\tilde{\theta}(V)$. For elemental metals it has been suggested that the increase in entropy from solid to liquid *at constant V* is roughly independent of V and is fairly universal across a wide range of elements.[3] Solid-liquid entropy differences for elements in the same column of the Periodic Table as Be (Mg and Ca) are around $(0.85-0.9)k_B$/atom (Ref. 3); we assume the identical difference for Be. If this difference is ΔS, then at high T for which the Mie-Grüneisen expression for F_i is valid, we have

$$\tilde{\theta}(V) = \theta_{solid}(V)\exp\left[-\frac{\Delta S}{3k_B}\right] \tag{11}$$

as long as F_e(solid)$=F_e$(liquid) in the neighborhood of the melt line. If ΔS is independent of V, then the V dependence of $\tilde{\theta}$ is entirely determined by the V dependence of θ_{solid}. Thus we choose the Grüneisen parameter of the liquid to be of the form $AV+B$, as we have for the solid phases. The melt line appearing in Fig. 6 was computed with two-phase simulations using the bcc phase; we then fix $\Delta S=0.87k_B$/atom and use $\theta_{\rm bcc}(V)$ for $\theta_{solid}(V)$, obtaining a form for $\tilde{\theta}(V)$ identical to that of Eq. (9) with $V_{\rm ref}$(liquid)$=7.62$ Å^3/atom, $\theta^{(0)}$(liquid)$=663.6$ K, A(liquid)$=0.131$ Å^{-3}, and B(liquid) $=0.364$. This choice then ensures that the change in entropy going from bcc to liquid is $0.87k_B$/atom at constant V, independent of V. Since $\theta_{\rm hcp}(V)$ is quite similar to $\theta_{\rm bcc}(V)$ on the whole, a very similar ΔS between hcp and liquid will be obtained as well.

With this choice of $\tilde{\theta}$, it is now possible to fix $F_0(V)$ for the liquid by requiring that the melt line be that as appearing in Fig. 6. In order for T_{melt} to be a concave down and monotonically increasing function of P, we must have: (1) V_0(liquid)$>V_0$(solid), (2) B_0(liquid)$<B_0$(solid), and (3) the obvious constraint that the minimum cold energy of the liquid is higher than that of the solid, so $\phi=E_0$(liquid) $-E_0$(solid)>0. Within our EOS model, the two lower-P melt points in Fig. 6 are within the hcp-stable region. Thus, we constrain the liquid cold curve by requiring that the hcp melt line goes through those two points, while the bcc melt line goes through the highest-P point.[36] Using the two-phase Maxwell construction to determine hcp-liquid and bcc-liquid phase lines, we arrive at a cold curve of the form: $F_0(V)=F_0^u(V)+F_0^{\rm break}(V)$. $F_0^u(V)$ is of the Vinet form[23] with parameters V_0(liquid)$=7.95$ Å^3/ atom, B_0(liquid)$=112$ GPa, B_1(liquid)$=3.64$, and $\phi=E_0$(liquid)$-E_0$(bcc)$=0.149$ eV/atom. $F_0^{\rm break}(V)=Au^n/(B+u^n)$, with $u=1-V_b/V$, and $A=-2.0$ eV, $B=5.0$, $n=3$, and $V_b=4.25$ Å^3/atom; $F_0^{\rm break}(V)$ is *only added* if $V>V_b$ and is *set to zero otherwise*. Note that we fixed the value of B_1 (liquid) to be the same as that of bcc

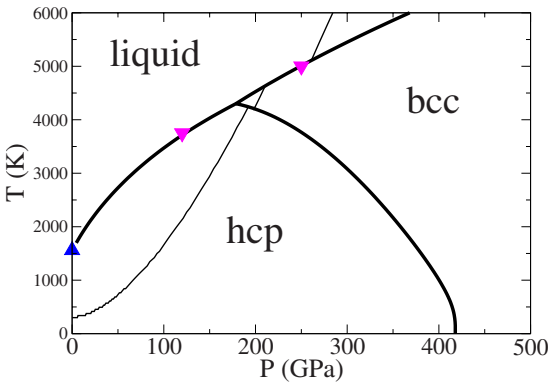

FIG. 7. (Color online) Phase diagram of Be from the EOS model. Upward triangle is the experimental ambient-pressure melt point (Ref. 10); downward triangles are results from two-phase simulations melting from bcc (Ref. 26). Thin lines denote the principal Hugoniot as computed by the EOS model.

for convenience. This choice of parameters defines $F_0(V)$ for the liquid. Together with $\tilde{\theta}(V)$ and the solid free energies discussed above, we obtain the phase diagram shown in Fig. 7. The melt lines from hcp and bcc are nearly identical, as evidenced by the absence of a prominent cusp in the melt line at the hcp-bcc-liquid triple point. This is due to the fact that hcp and bcc free energies are so remarkably similar, as we noted above.

Figure 8 shows energy and pressure isotherms for liquid Be as computed by the free energy model, together with select results obtained by performing *ab initio* MD simulations. For these simulations, we placed 512 Be atoms in a box with periodic boundary conditions and used the QBOX code[37] with Γ-only k-point sampling to compute energy and pressure at the desired densities and temperatures by simulating for up to several picoseconds. Time steps were chosen to be 1 fs and we used a velocity-scaling thermostat with a response time of 100 fs. Note that the agreement between E and P as computed in the MD and E and P as predicted by the liquid free energy model is quite good.[38] This suggests that the liquid model is relatively accurate and that the basic assumptions embodied in the model, such as the use of Eqs. (10) and (11), are reasonable. We emphasize that the *ab initio* MD calculations of E and P for liquid Be were *not* used to fit the liquid free energy model.

B. High-T liquid: Plasma

Above $k_BT=2$ eV, we use a global EOS model similar to QEOS (Ref. 39) for generating the EOS of the liquid. In QEOS, the free energy is partitioned as in Eq. (1). $F_0(V)$ is of a form similar to what we have described above, only defined over a much wider range of V. The ion-thermal term is constructed to have a specific heat which is equal to $3k_B$ at $T_{melt}(V)$ and drops to the ideal gas value of $3/2k_B$ according to the scaling law $[T_{melt}(V)/T]^{1/3}$, where $T_{melt}(V)$ is the melt temperature as predicted by the Lindemann law.[3] The use of the Lindermann law requires that the Grüneisen parameter of the solid be specified as a function of V. Our model for $\gamma_{solid}(V)$ is a piecewise linear function which closely resembles the phase dependent γ we have determined above for Be. Care must be taken when constructing the electron-thermal term at high T, as this term becomes the dominant contributor as T/T_{melt} becomes very large and ionization plays a role. Fortunately, it is in this regime that the details of chemical bonding prevalent in the solid and low-T liquid become less important. Thus, we use an average-atom-in-jellium model for $F_e(V,T)$, in which hot Be is modeled as a representative ion placed in a homogeneous electron-gas background. An early incarnation of this model, Inferno,[40] solved this problem within a DFT framework using the LDA. We use essentially the same prescription here, though with an upgraded numerical package with enhanced capabilities to track atomic resonances, known as Purgatorio.[18] In this way, we are able to include the effects of inner shell ionization on the EOS, in which the basic thermodynamic variables such as E and P change dramatically as an electron, once bound and localized to an ion, becomes "free" and moves into the jellium continuum.

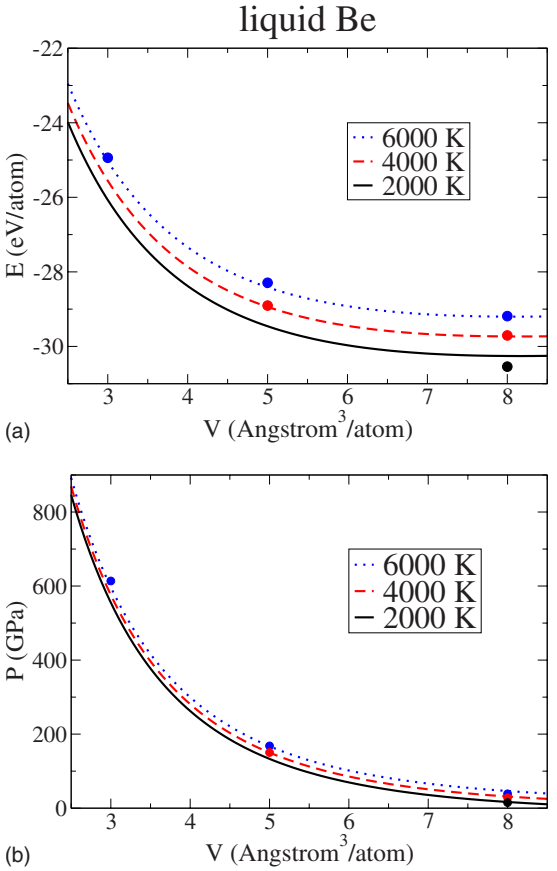

FIG. 8. (Color online) Internal energy and pressure isotherms in the liquid. Lines are the results of the liquid free energy model; dots are the results from *ab initio* MD.

This global EOS model applies over a much wider range of density, temperature, and pressure than the three-phase EOS. It is therefore necessary to embed the more detailed three-phase EOS model within the wider-range global model while maintaining thermodynamic consistency in the overall tabulated EOS. This was done in three steps. First, the global EOS was constructed to agree as closely as possible with the pressure and energy isotherm at a temperature of 2 eV from

the smaller-range three-phase EOS. After applying an energy shift to align the energy zero values in the models, agreement was achieved at the high-density region, but there was still some discrepancy at the low density end. The second step eliminated this discrepancy by smoothly and monotonically interpolating between the low-T model and the high-T model over a temperature range of 1.4 eV. Finally, a similar interpolation procedure was used to smooth the transition as a function of density, both at the low density ($0.8-1.66$ g/cm^3) and at high-density ($14.96-25.1$ g/cm^3) ends of the three-phase model. The interpolation started at the boundary of the three-phase model and modified only the values of the EOS associated with the global model. This procedure resulted in a global equation of state that obeys the thermodynamic constraint $dE/dT>0$ everywhere.

C. Discussion of principal shock Hugoniot

Returning to the lower-T phase diagram, the prediction of the hcp-bcc phase line, together with its relation to the Be melt curve, has implications for the interpretation of dynamic high-pressure experiments performed on Be. If Be is subjected to a planar one-dimensional shock, the locus of accessible final states will lie along the principal Hugoniot curve,[8] which we calculate and display as the thin lines in Fig. 7.[41] Note the discontinuities in the Hugoniot when traversing the phase boundaries, a reflection of the fact that each phase possesses a distinct free energy function. In particular, there is a very small discontinuity going from hcp$\rightarrow$bcc. This is due to the very small entropy difference between the two solid phases. There is a larger difference, however, between the solid and liquid portions of the Hugoniot. This is due to the larger entropy difference ($\sim 0.9k_B$/atom) we assumed between solid and liquid.

A key question is whether or not it is possible to shock into the bcc phase prior to melting, starting from the ambient hcp initial state. Our work suggests that a definitive answer to this question is likely to be difficult to obtain from our predictions alone. The reason is that uncertainties in the hcp-bcc phase line together with uncertainties in the melt curve provide a wide range of possible shock melt scenarios. For example, in our EOS model, the hcp-bcc-liquid triple point shown in Fig. 7 is right in the neighborhood of the point at which the principal Hugoniot crosses the melt curve on the solid side just above 200 GPa. Even though our scenario predicts a small region of bcc stability along the Hugoniot, a small change in the position of the triple point could eliminate this region entirely *even if the Hugoniot remains unchanged*. Therefore, all we can say at present is that we would predict at most a small portion of the principal Hugoniot to lie in a bcc-stable region.[42]

Figure 9 shows the high-P and -T portions of the principal Hugoniot in the (ρ,P) plane as computed with the Purgatorio-based global EOS. The small kink at a density just under 6 g/cm^3 corresponds to a temperature of roughly 2 eV and is a result of the imperfect join between the lower-T three-phase and higher-T plasma-based models. The maximum compression reached along the principal Hugoniot is just over 8.5 g/cm^3, larger than that predicted by the Thomas-Fermi electron-thermal contribution as in the original QEOS work.[39] The sharp turnaround in the P versus ρ Hugoniot curve is a result of the ionization of the $1s^2$ core and corresponds to a temperature of roughly 10^6 K. In addition to capturing this ionization physics, the Purgatorio model uses a fully relativistic treatment for the electrons at all temperatures. This is responsible for the density increase again at very high pressures above 10^6 GPa, resulting ultimately in a limiting value of seven times the initial density.

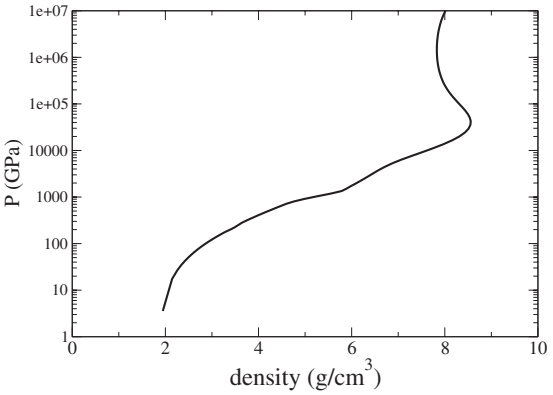

FIG. 9. Principal Hugoniot of Be in the plasma regime as calculated by the global EOS model with an electron-thermal term provided by Purgatorio.[18]

IV. CONCLUSIONS

We have constructed a multiphase EOS for Be using phase-dependent free energy models constrained by *ab initio* calculations. The hcp-bcc phase line was computed to be in rough agreement with previous theoretical work[5,6,14] in which the ambient-pressure extrapolation of the phase boundary is above the melt curve. This is in stark contradiction to the early experimental findings[10] but in agreement with more recent results.[13] We have also investigated $T=0$ internal energies of Be along the Burgers path connecting hcp to bcc, from which we demonstrated that the energy well around bcc is very flat, and the barrier separating hcp and bcc is very small. The liquid EOS was constrained by our knowledge of the solid EOS and the melt curve, together with atom-in-plasma calculations to address very high temperatures. Our Be EOS model is suitable for use in calculations of material behavior in extreme conditions.

ACKNOWLEDGMENTS

We thank M. Desjarlais, C. W. Greeff, D. A. Young, P. Soderlind, D. Orlikowski, A. Correa, S. P. Rudin, W. J. Evans, M. J. Lipp, and R. M. M. Wentzcovitch for helpful discussions. This work was performed under the auspices of the U.S. Department of Energy at the Lawrence Livermore National Laboratory under Contract No. DE-AC52-07NA27344.

[1] D. A. Young, *Phase Diagrams of the Elements* (University of California Press, Berkeley, 1991).
[2] R. Boehler, Nature (London) **363**, 534 (1993).
[3] D. C. Wallace, *Statistical Physics of Crystals and Liquids* (World Scientific, Singapore, 2003).
[4] M. Ekman, B. Sadigh, K. Einarsdotter, and P. Blaha, Phys. Rev. B **58**, 5296 (1998).
[5] S. P. Rudin, M. D. Jones, and J. D. Johnson, *20th AIRAPT Conference Proceedings, Karlsruhe, 2005*, edited by E. Dinjus and N. Dahmen (Forschungszentrum Karlsruhe, Germany, 2005), p. O058.
[6] G. Robert and A. Sollier, J. Phys. IV **134**, 257 (2006).
[7] D. S. Clark, S. W. Haan, and J. D. Salmonson, Phys. Plasmas **15**, 056305 (2008).
[8] M. A. Meyers, *Dynamic Behavior of Materials* (Wiley, New York, 1994).
[9] In principle, dynamic compression could involve time scales fast enough so that equilibrium is not reached, in which case detailed kinetic models would have to be employed. We ignore these effects in this work.
[10] M. Francois and M. Contre, in *Conference Internationale sur la Metallurgie du Beryllium* (Universite de France, Grenoble, Paris, 1965).
[11] A. Abey, Lawrence Livermore National Laboratory Report No. UCRL-53567, 1991.
[12] W. J. Evans, M. J. Lipp, H. Cynn, C. S. Yoo, M. Somayazulu, D. Häusermann, G. Shen, and V. Prakapenka, Phys. Rev. B **72**, 094113 (2005).
[13] W. J. Evans and M. J. Lipp (private communication).
[14] G. Robert, A. Sollier, and Ph. Legrand, in *Shock Compression of Condensed Matter—2007*, edited by Mark Elert, Michael D. Furnish, Ricky Chau, Neil Holmes, and Jeffrey Nguyen, AIP Conf. Proc. No. 955 (AIP, New York, 2007), p. 97.
[15] K. Kadas, L. Vitos, B. Johansson, and J. Kollar, Phys. Rev. B **75**, 035132 (2007).
[16] E. D. Chisolm and D. C. Wallace, J. Phys.: Condens. Matter **13**, R739 (2001).
[17] E. D. Chisolm, S. D. Crockett, and D. C. Wallace, Phys. Rev. B **68**, 104103 (2003).
[18] B. Wilson, V. Sonnad, P. Sterne, and W. Isaacs, J. Quant. Spectrosc. Radiat. Transf. **99**, 658 (2006).
[19] J. P. Perdew, K. Burke, and M. Ernzerhof, Phys. Rev. Lett. **77**, 3865 (1996).
[20] QUANTUM-ESPRESSO is a community project for high-quality quantum-simulation software based on density-functional theory and coordinated by Paolo Giannozzi (see http://www.quantum-espresso.org and http://www.pwscf.org).
[21] N. Troullier and J. L. Martins, Phys. Rev. B **43**, 1993 (1991).
[22] L. Kleinman and D. M. Bylander, Phys. Rev. Lett. **48**, 1425 (1982).
[23] P. Vinet, J. H. Rose, J. Ferrante, and J. R. Smith, J. Phys.: Condens. Matter **1**, 1941 (1989).
[24] We fit the cold curve over a wide range of volumes ($\sim$3–8 Å^3/atom), so we do not expect our extracted cold curve parameters (V_0, B_0, B_0', E_0) to be the optimal ones for describing the behavior *right in the neighborhood of* V_0 (i.e., near ambient conditions). Rather, they are a set of parameters which give a good *global* fit over the wide range of volumes considered.
[25] M. Y. Chou, P. K. Lam, and M. L. Cohen, Phys. Rev. B **28**, 4179 (1983).
[26] A. Trave, T. Ogitsu, E. Schwegler, L. X. Benedict, and G. Galli (unpublished).
[27] E. C. Bain, Trans. AIME **70**, 25 (1924).
[28] W. G. Burgers, Physica (Utrecht) **1**, 561 (1934).
[29] D. C. Wallace, *Thermodyamics of Crystals* (Dover, New York, 1998).
[30] X. Gonze and C. Lee, Phys. Rev. B **55**, 10355 (1997).
[31] *Chemical Rubber Company Handbook of Chemistry and Physics*, 79th ed., edited by D. R. Lide (CRC, Boca Raton, FL, 1998).
[32] We have not explored the possibility that bcc may be stabilized by higher temperatures. See Ref. 15 for a study arguing that bcc is stabilized by a softening in the elastic constants at ambient volume.
[33] F. E. Simon and G. Z. Glatzel, Z. Anorg. Allg. Chem. **178**, 309 (1929).
[34] In addition, our preliminary studies of $\langle r^2 \rangle$, the thermally averaged mean squared displacement of atoms, using *ab initio* MD, have failed to uncover any significant deviations from the values predicted by quasiharmonic theory. We therefore do not expect anharmonicity in hcp and bcc Be to affect the ionic entropy, and thus relative phase stability, in a serious way. Calculations of $\langle r^2 \rangle$, however, pose an exceptional challenge for MD with finite-sized cells since $\langle r^2 \rangle$ is particularly sensitive to the low-energy long-wavelength acoustic modes, as well as to the k-point sampling of the electronic states used in the self-consistent field calculation. L. X. Benedict, M. P. Desjarlais, T. Ogitsu, and E. Schwegler (unpublished).
[35] A. A. Correa, L. X. Benedict, D. A. Young, E. Schwegler, and S. A. Bonev, Phys. Rev. B **78**, 024101 (2008).
[36] The two-phase simulation MD melt point at $P \sim 120$ GPa was computed by melting out of bcc not hcp. In principle then, we should fit the liquid $F_0(V)$ by constraining this point to be on the bcc melt curve even though we predict it to lie in the stability field of hcp. However, all of our candidate parametrizations of the liquid free energy show the hcp and bcc melt curves to be very close at this (P,T).
[37] F. Gygi, QBOX is a C++/MPI scalable parallel implementation of first-principles molecular dynamics (FPMD) based on the plane-wave pseudopotential formalism developed by (http://eslab.ucdavis.edu/).
[38] At large V, the agreement as exhibited in Fig. 8 is not as good as at smaller V. This may be due to the fact that the liquid EOS was determined by using the bcc phase as a reference. As noted above, the bcc free energy is really an extrapolation in this region, owing to its mechanical instability at large V. Also, we note that our use of only the Γ point in the *ab initio* MD produces errors of roughly 0.1 eV/atom in E and 20 GPa in P for bcc Be when using MD cells in this size range.
[39] R. M. More, K. H. Warren, D. A. Young, and G. B. Zimmerman, Phys. Fluids **31**, 3059 (1988).
[40] D. A. Liberman, Phys. Rev. B **20**, 4981 (1979).
[41] Our calculation of the principal Hugoniot in the (P,V) plane is essentially identical to that displayed in Ref. 14. Provided that V_0 is shifted appropriately to coincide with the measured density at ambient conditions, the principal Hugoniot overlays the experimental points as shown in Ref. 14.
[42] This statement is consistent with recent calculations and measurements by Desjarlais and Knudsen, March APS08, abstract B13.00002.